Author/s:
Li, S;Ju, Y;Zhou, J;Noi, KF;Mitchell, AJ;Zheng, T;Kent, SJ;Porter, CJH;Caruso, F

Title:
Quantitatively Tracking Bio-Nano Interactions of Metal-Phenolic Nanocapsules by Mass Cytometry

Date:
2021-08-04

Citation:
Li, S., Ju, Y., Zhou, J., Noi, K. F., Mitchell, A. J., Zheng, T., Kent, S. J., Porter, C. J. H. & Caruso, F. (2021). Quantitatively Tracking Bio-Nano Interactions of Metal-Phenolic Nanocapsules by Mass Cytometry. ACS Applied Materials and Interfaces, 13 (30), pp.35494-35505. https://doi.org/10.1021/acsami.1c09406.

Quantitatively Tracking Bio–Nano Interactions of Metal–Phenolic Nanocapsules by Mass Cytometry

Shiyao Li,[#,‡] Yi Ju,[#,‡,†] Jiajing Zhou,[#,¶] Ka Fung Noi,[○] Andrew J. Mitchell,[§] Tian Zheng,[§] Stephen J. Kent,[^,⊥,] Christopher J. H. Porter,[○,*] and Frank Caruso[#,*]*

[#]ARC Centre of Excellence in Convergent Bio-Nano Science and Technology, and the Department of Chemical Engineering, The University of Melbourne, Parkville, Victoria 3010, Australia

[○]Drug Delivery, Disposition and Dynamics, Monash Institute of Pharmaceutical Sciences, Monash University (Parkville Campus), 381 Royal Parade, Parkville, Victoria 3052, Australia

[§]Department of Chemical Engineering, Materials Characterisation and Fabrication Platform, The University of Melbourne, Parkville, Victoria 3010, Australia

[^]Department of Microbiology and Immunology, Peter Doherty Institute for Infection and Immunity, The University of Melbourne, Parkville, Victoria 3010, Australia

[⊥]ARC Centre of Excellence in Convergent Bio-Nano Science and Technology, Department of Microbiology and Immunology, The University of Melbourne, Parkville, Victoria 3010, Australia

KEYWORDS: metal–phenolic networks, nanocapsules, size-dependent bio–nano interactions, human full blood assays, biodistribution

Abstract

Polymer nanocapsules, with a hollow structure, are increasingly finding widespread use as drug delivery carriers; however, quantitatively evaluating the bio–nano interactions of nanocapsules remains challenging. Herein, poly(ethylene glycol) (PEG)-based metal–phenolic network (MPN) nanocapsules of three sizes (50, 100, and 150 nm) are engineered via supramolecular template-assisted assembly and the effect of nanocapsule size on bio–nano interactions is investigated using in vitro cell experiments, ex vivo whole blood assays, and in vivo rat models. To track the nanocapsules by mass cytometry, a preformed gold nanoparticle (14 nm) is encapsulated into each PEG–MPN nanocapsule. The results reveal that decreasing the size of the PEG–MPN nanocapsules from 150 to 50 nm leads to reduced association (up to 70%) with phagocytic blood cells in human blood and prolongs the elimination half-life (increased from 1 to 4 h) in rat models. The findings provide insights into MPN-based nanocapsules and represent a platform for studying bio–nano interactions.

Introduction

Hollow nanospheres, or nanocapsules, have drawn scientific attention owing to their various potential applications, including drug and gene delivery, catalysis, cosmetics, and hydrogen production and storage.[1–4] The physiochemical properties of nanocapsules can be tuned to achieve high drug loading efficiency and controlled cargo release, which makes them promising drug delivery carriers.[5] The delivery efficiency of nanocarriers is largely influenced by their physicochemical properties, including size,[6–9] shape,[9–12] charge,[13] and surface chemistry.[14]

Particle size has been reported to be a key parameter, and it is widely accepted that nanocarriers larger than 200 nm in diameter are rapidly cleared by the mononuclear phagocyte system (MPS), whereas those smaller than 5 nm are filtered out by the kidneys.[15] Accordingly, the desirable size range of nanocarriers for drug delivery is considered to be 20–150 nm.[16] For instance, Wang et al. synthesized micelles using amphiphilic block copolymers with sizes ranging from 20 to 300 nm, and the effect of micelle size on blood circulation and tumor penetration was studied. The micelles with sizes of 100–160 nm displayed longer circulation time and tumor accumulation than the smaller (30 nm) and larger (300 nm) micelles.[8] However, there remains a lack of systematic studies on the size effect of monodisperse nanocapsules on bio–nano interactions, which can be partly attributed to the challenges to maintain colloidal stability and achieve size control when synthesizing nanocapsules with diameters of less than 200 nm.

The development of metal–phenolic networks (MPNs), a class of hybrid coordination networks, has allowed for a simple, fast, and controllable method to deposit nanofilms on a broad range of substrates for material synthesis.[17] The films are assembled through coordination bonding between polyphenols (e.g., tannic acid (TA)) and metal ions (e.g., Fe^{3+}). By coating MPN films on nano/microparticle templates and subsequent removal of the template, MPN nano- and microcapsules can be obtained.[18] Poly(ethylene glycol) (PEG)-based MPN systems were subsequently developed by coordinating metal ions with PEG–polyphenol.[19,20] PEG, which is approved by the US Food and Drug Administration, is widely used for modification during nanoparticle preparation.[21] PEG can improve the hydrophilicity of nanoparticles and reduce their interactions with proteins and cells, thus endowing nanoparticles with stealth properties.[22–26] Our previous studies have shown that PEG–MPN particles exhibit resistance to nonspecific protein adsorption and cellular association,[19] and good biocompatibility and biodegradability in vivo.[27]

However, engineering PEG–MPN capsules on the nanoscale with controllable size is a challenge, and the weak intrinsic fluorescence of the capsules adds to the difficulty of tracking them in vitro, ex vivo, and in vivo.

Currently, the detection and tracking of nanoparticles is typically performed using either fluorescent agents (e.g., the organic dye fluorescein isothiocyanate) or exogenous radioactive isotopes (e.g., ^{125}I, ^{64}Cu, ^{177}Lu).[28–30] However, the common challenges of fluorescence-based labeling arise because of autofluorescence from biological samples, which can interfere with the detection and quantification of the nanoparticles. Moreover, the broad absorption and emission spectra of fluorescence limit the detection accuracy and the number of fluorophores that can be used simultaneously.[31] In contrast, the use of radioactive isotopes requires specialized knowledge and equipment, careful safety considerations, and regulated laboratory space.[32] In addition, exogenous fluorescence or radioactive labeling can potentially change the surface properties of nanoparticles and subsequently alter their biological behaviors. The exogenous labels can also possibly break away from the nanoparticles, thereby potentially resulting in misrepresentation of the behaviors of the nanoparticles.[33] The use of metal nanoparticles, e.g., Ag, Au, Pt, and Pd, which can be detected by inductively coupled plasma mass spectrometry (ICP-MS) or cytometry by time-of-flight (CyTOF), offers an alternative approach for tracking nanocarriers in biological environments.[14,34–38]

Herein, we prepared PEG–MPN nanocapsules of different sizes (50, 100, and 150 nm) through template-assisted assembly and investigated their size effect on immune cell interactions in human blood and biodistribution in rats (Scheme 1). A 14 nm Au nanoparticle (AuNP) was incorporated into the supramolecular template, thereby serving as a stable tracking agent for mass cytometry-based cell experiments and in vivo studies. By tuning the size of the PEG–MPN nanocapsules, the

circulation time of the nanocapsules could be prolonged, where the sub-100 nm PEG–MPN nanocapsules demonstrated lower immune cell association in blood and longer circulation in vivo than the larger nanocapsules (150 nm) studied.

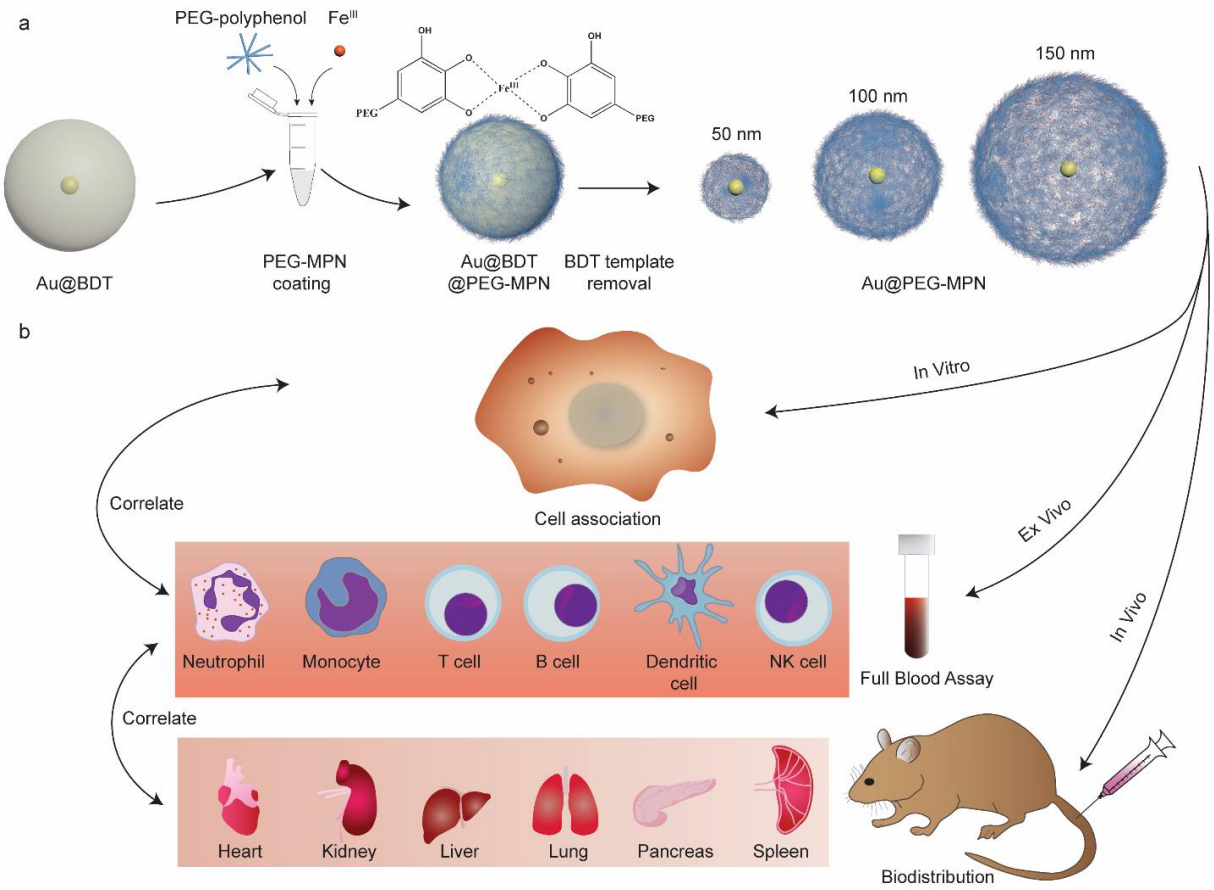

Scheme 1. (a) Preparation of AuNP-encapsulated PEG–MPN core–shell nanoparticles and nanocapsules of three different sizes. (b) In vitro cell association assay, ex vivo whole blood assay, and in vivo experiment using rat models were designed to assess the bio–nano interactions of the PEG–MPN nanocapsules.

Results and Discussion

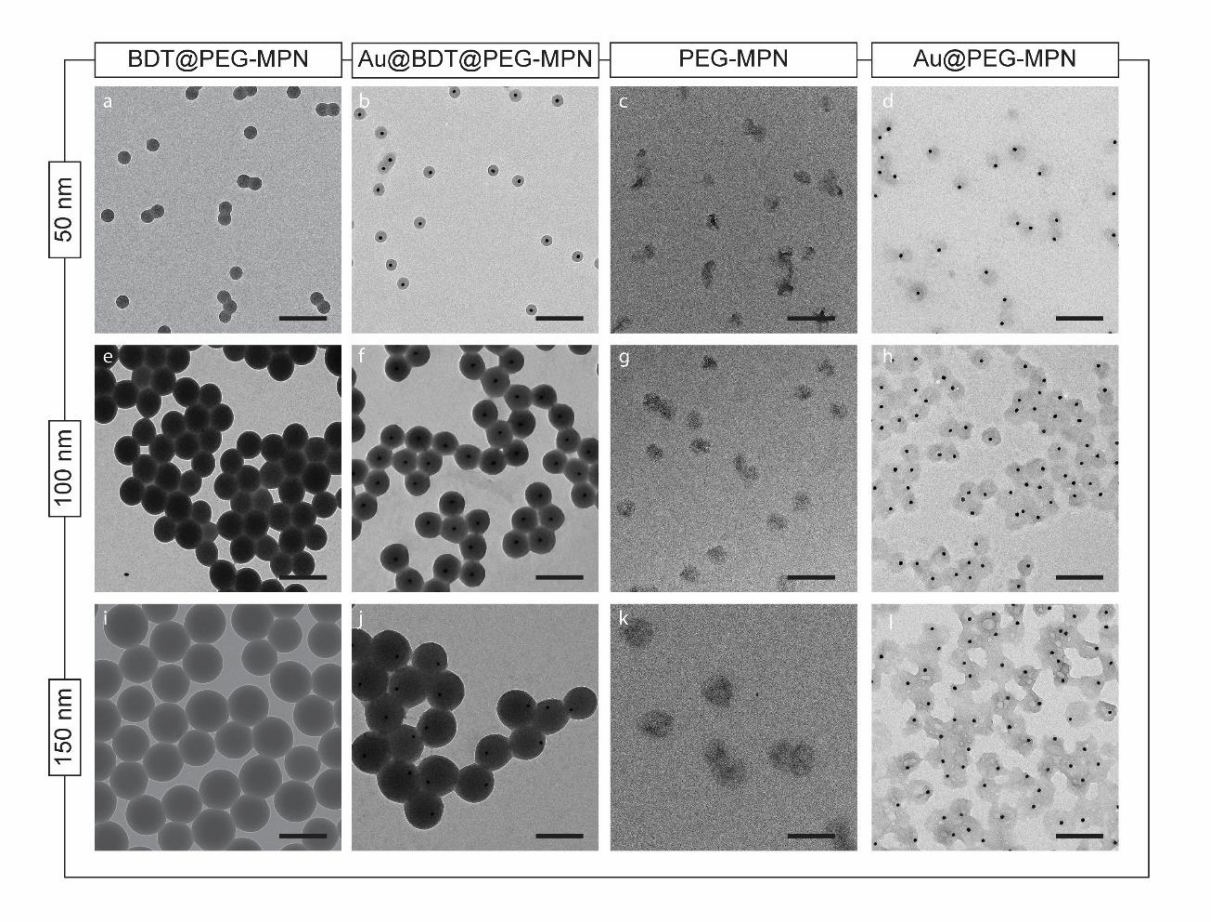

Figure 1. TEM images of (a,e,i) BDT@PEG–MPN core–shell nanoparticles, (b,f,j) Au@BDT@PEG–MPN core–shell nanoparticles, (c,g,k) PEG–MPN nanocapsules, and (d,h,l) Au@PEG–MPN nanocapsules of three sizes 50 nm (a–d), 100 nm (e–h), and 150 nm (i–l). PEG–MPN and Au@PEG–MPN nanocapsules were obtained after BDT removal. Scale bars are 200 nm.

Synthesis and Characterization of PEG–MPN and Au@PEG–MPN Nanocapsules. PEG–MPN and Au@PEG–MPN nanocapsules of different sizes were prepared via a template-assisted assembly process using benzene-1,4-dithiol (BDT) particles and AuNP-encapsulated BDT particles as templates, respectively. BDT of three different sizes (50, 100, and 150 nm) were synthesized based on a reported method.[39] Au@BDT template particles were obtained by

encapsulating a 14 nm AuNP in each BDT particle during synthesis. The spherical shape and uniform size distribution of the BDT particles, as well as the encapsulation of a single 14 nm AuNP in each BDT particle were observed from the transmission electron microscopy (TEM) images in Figure S1. For MPN formation, a PEGylated phenolic ligand (PEG–gallol) was synthesized by conjugating 8-arm-PEG-succinimidyl glutarate with 5-hydroxydopamine via amide bonds, where the terminal galloyl groups can coordinate to Fe^{III} ions. All eight PEG end-groups were conjugated with the galloyl moieties, as confirmed by ^{1}H NMR spectroscopy (Figure S2).

To prepare the PEG–MPN nanocapsules, PEG–galloyl was added to the BDT nanoparticles, followed by addition of $FeCl_3$ aqueous solution and subsequent raising of the pH to 8.5 with 3-(*N*-morpholino)propanesulfonic acid (MOPS) buffer (Scheme 1). This product is referred to as PEG–MPN-coated BDT (BDT@PEG–MPN) core–shell nanoparticles (Figure 1a,e,i). After dissolving the BDT templates with dimethylformamide (DMF), PEG–MPN nanocapsules were obtained (Figure 1c,g,k). To prepare the Au@PEG–MPN nanocapsules, BDT template nanoparticles containing encapsulated AuNPs (Au@BDT nanoparticles) were used instead as templates. The core–shell nanoparticles with the individually encapsulated 14 nm AuNPs (Au@BDT@PEG–MPN) are shown in Figure 1b,f,i and the Au@PEG–MPN nanocapsules, following BDT template removal, are shown in Figure 1d,h,l. As observed from the TEM images, the PEG–MPN nanocapsules exhibited lower contrast than the BDT@PEG–MPN core–shell nanoparticles (Figure 1), demonstrating the removal of the BDT templates.

The Au@BDT@PEG–MPN core–shell nanoparticles and Au@PEG–MPN nanocapsules (prepared from PEG with a molecular weight of 40 kDa and respectively referred to as Au@BDT@40k-PEG–MPN and Au@40k-PEG–MPN) were well dispersed in aqueous solution, displaying a uniform size distribution as determined from nanoparticle tacking analysis (NTA)

(Figure 2a–c). The average size of the different types of Au@BDT@40k-PEG–MPN core–shell nanoparticles was 42.8 ± 0.2, 106.0 ± 1.7, and 148.1 ± 8.8 nm, respectively (Table S1). After BDT core template removal, the obtained Au@40k-PEG–MPN capsules featured average sizes of 53.8 ± 6.5, 100.1 ± 0.3, and 132.7 ± 3.5 nm, respectively (Table S1). Hereafter, for simplicity, the size of the core–shell nanoparticles and nanocapsules is referred to according to the size of the BDT template (i.e., 50, 100, and 150 nm) used during preparation. Incubation of the 50, 100, and 150 nm Au@40k-PEG–MPN nanocapsules in human plasma for 12, 24, 48, and 72 h confirmed the stability of the nanocapsules, as indicated by the minimal changes observed in the size distribution (assessed by NTA) of the nanocapsules within 24 h (Figures S3–S5). TEM analysis also showed that the AuNPs remained encapsulated within the Au@40k-PEG–MPN capsules after incubation for 48 h in human plasma (Figure S4). Atomic force microscopy (AFM) measurements performed in on air-dried samples (i.e. "dry state") on the 150 nm (148.1 ± 8.8 nm) Au@BDT@40k-PEG–MPN core–shell nanoparticles revealed that the thickness of the nanoparticles was around 136 nm (Figure 2d, Table S1), which is comparable to the size measurement in solution. In contrast, the thickness of the 150 nm (132.7 ± 3.5 nm) Au@40k-PEG–MPN nanocapsules was around 10 nm in the "dry state" (Figure 2e, Table S1), corresponding to a single shell thickness of 5 nm. This is approximately 27-fold less than the diameter of the nanocapsules in aqueous solution, demonstrating the hollow feature of the nanocapsules.

The ultraviolet–visible (UV–vis) absorption spectra of the 100 nm Au@40k-PEG–MPN nanocapsules showed the presence of a ligand-to-metal charge transfer band in the range of 492–575 nm (Figure 2f), which indicates the successful formation of bis- and tris-complexes between gallol and Fe^{3+}, of which the absorption peaks are located at 575 and 492 nm, respectively.[19] A UV absorbance peak near 520 nm was also observed, which is associated with 14 nm AuNPs, as

consistent with a previous study.[40] Microelectrophoresis measurements of the Au@BDT@40k-PEG–MPN core–shell nanoparticles and Au@40k-PEG–MPN nanocapsules (Figure 2g) showed that after coating the templates with PEG–MPN, the ζ-potential of the particles reduced from −38.3 ± 2.4 mV (template particles) to approximately −4 mV (Table S1). The ζ-potential values remained unchanged after template removal. This result is comparable with previous studies that have reported the ζ-potential of PEG–MPN emulsions to be around −10 mV.[27] Successful removal of Au@BDT templates was also confirmed by X-ray photoelectron spectroscopy (XPS) (Figure S7), as indicated by the absence of S 2s signal at ~226 eV and S 2p signal at ~165 eV in the XPS pattern of the 100 nm Au@40k-PEG–MPN nanocapsules; these signals were present in the 100 nm Au@BDT nanoparticles and Au@BDT@40k-PEG–MPN core–shell nanoparticles.

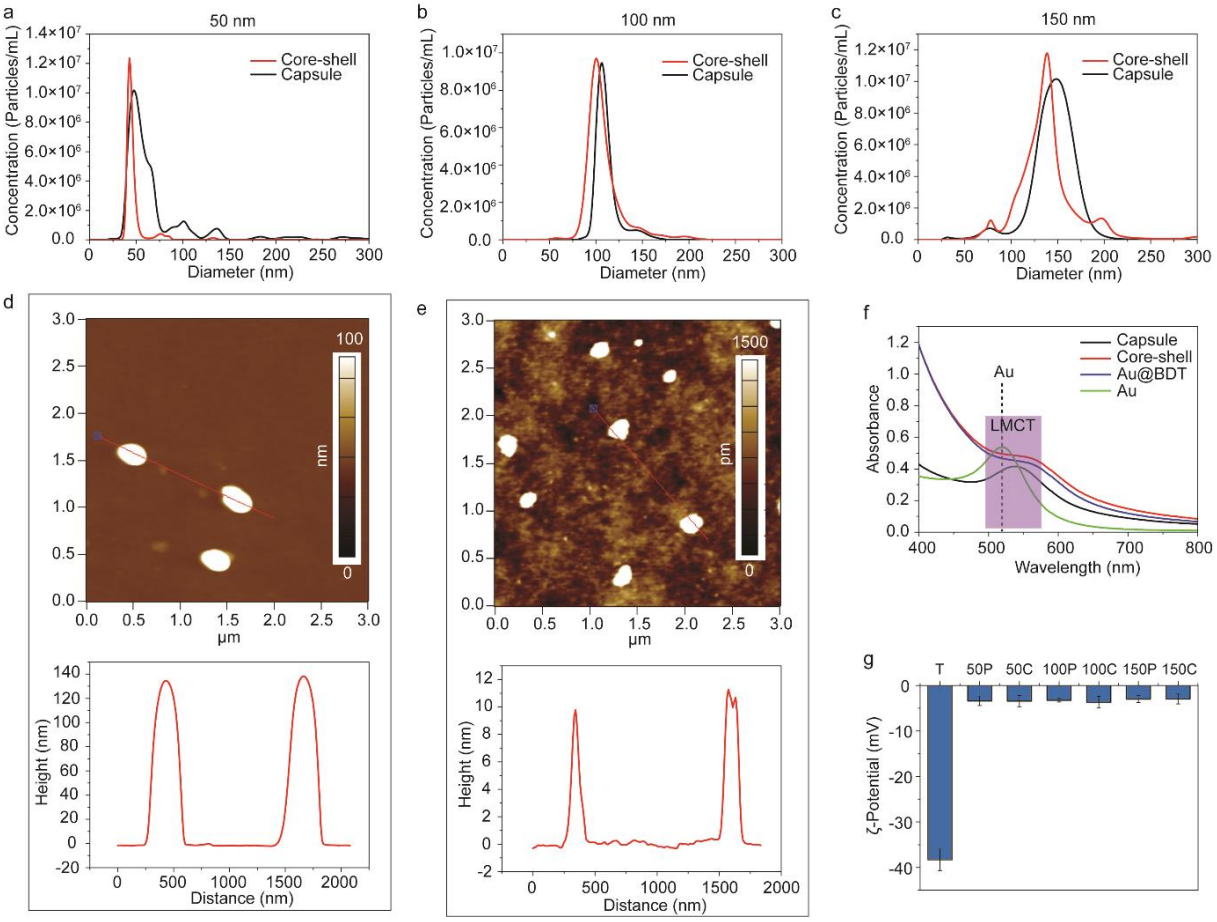

Figure 2. (a–c) Size distribution of Au@BDT@40k-PEG–MPN core–shell nanoparticles and Au@40k-PEG–MPN nanocapsules determined by NTA. AFM measurements of the 150 nm (d) Au@BDT@40k-PEG–MPN core–shell nanoparticles and (e) Au@40k-PEG–MPN nanocapsules. (f) UV–vis absorption spectra of AuNPs, and 100 nm Au@BDT, Au@BDT@40k-PEG–MPN core–shell nanoparticles and Au@40k-PEG–MPN nanocapsules measured in solution. (g) ζ-potential of 100 nm Au@BDT template (T), and Au@BDT@40k-PEG–MPN core–shell nanoparticles (*x*P) and Au@40k-PEG–MPN nanocapsules (*x*C), where *x* (i.e., 50, 100, and 150) represents the size of the particles and capsules in nanometers.

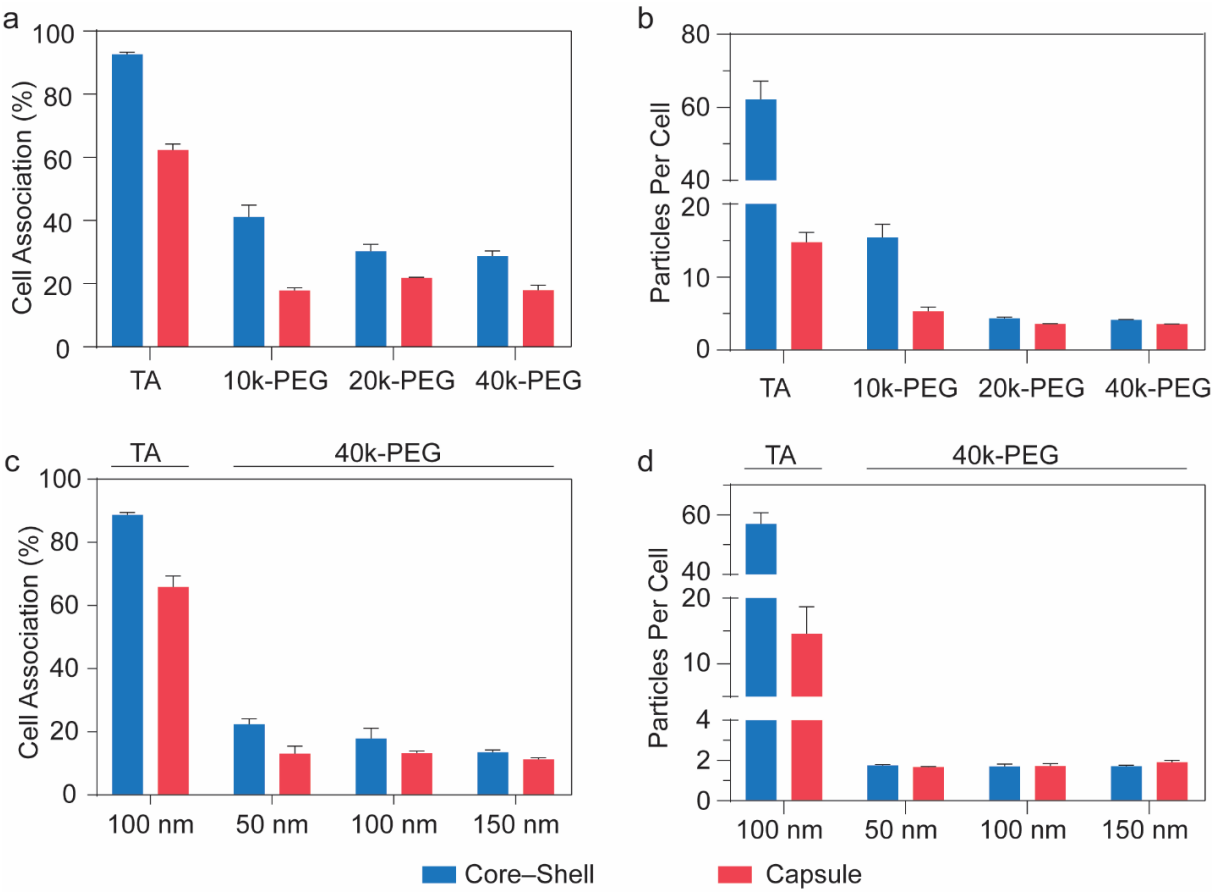

Figure 3. (a,b) Association (measured as % and number of particles per cell) of 100 nm Au@BDT@PEG–MPN core–shell nanoparticles and Au@PEG–MPN nanocapsules prepared with different PEG molecular weights (10, 20, and 40 kDa) with RAW 264.7 cells after incubation

for 24 h at 37 °C at a cell-to-particle ratio of 1:1000. (c,d) Association (measured as % and number of particles per cell) of Au@BDT@40k-PEG–MPN core–shell nanoparticles and Au@40k-PEG–MPN nanocapsules of different sizes (50, 100, and 150 nm) with RAW 264.7 cells after incubation for 24 h at 37 °C at a cell-to-particle ratio of 1:1000. Au@BDT@TA–Fe MPN core–shell particles and Au@TA–Fe MPN capsules (denoted as "TA") are included as a positive control. Cell association (%) in (a,c) refers to the proportion of RAW 264.7 cells with positive Au signals above background. The number of particles per cell in (b,d) refers to the average number of particles associated with RAW 264.7 cells, which is calculated based on the median Au signals of the nanoparticles that display association with the cells. Calculation details of single nanoparticle Au intensity are included in the caption of Figure S9. Data are shown as the mean ± standard deviation (SD) of three independent experiments, with 10000 cells analyzed for each experimental condition studied. Full statistical analysis is presented in Figures S10 and S11.

In Vitro Assessment of Particle Cytotoxicity and Interactions with Immortalized Cell Lines. The cytotoxicity of the Au@BDT@40k-PEG–MPN core–shell nanoparticles, and Au@40k-PEG–MPN and 40k-PEG–MPN nanocapsules was assessed by incubating the particles with a murine macrophage (RAW 264.7) cell line at varying cell-to-particle ratios for 48 h. As shown in Figure S8, the core–shell nanoparticles and nanocapsules had negligible influence on cell viability. To investigate the stealth properties of the Au@BDT@40k-PEG–MPN core–shell nanoparticles and Au@40k-PEG–MPN nanocapsules, in vitro cell association assays were performed using RAW 264.7 cells. As a positive control, 100 nm Au@TA–Fe MPN nanocapsules (PEG–gallol was replaced with TA during capsule synthesis) were used. Cellular association could be tracked by mass cytometry (also known as (CyTOF)) as AuNPs were encapsulated within the PEG–MPN nanocapsules. PEG is well known to hinder the opsonization of proteins;[21]

furthermore, the length and molecular weight of PEG can influence this process.[6,41] To assess the effect of PEG molecular weight on protein opsonization, 100 nm Au@BDT@PEG–MPN core–shell nanoparticles and Au@PEG–MPN nanocapsules prepared with different PEG molecular weights (10, 20, or 40 kDa) were examined (Figure 3a,b). The cellular association results showed that after incubation for 24 h, the Au@PEG–MPN nanocapsules had significantly lower association than the Au@BDT@PEG–MPN core–shell nanoparticles or Au@TA–Fe MPN nanocapsules ("TA" control) irrespective of the PEG molecular weight (Figure 3a, Figure S10). As the PEG molecular weight of the core–shell particles increased from 10 to 40 kDa, the absolute number of particles interacting with the cells further reduced from 15 particles per cell to fewer than 5 particles per cell (Figure 3b), suggesting improved stealth properties of the PEG–MPN coating when using 40k-PEG–gallol as the building blocks. Thus, using 40 kDa PEG–gallol as building blocks, we studied the particle size effect on particle–immune cell interactions (Figure 3c,d). The Au@40k-PEG–MPN nanocapsules displayed minimal cell association with RAW 264.7 cells (fewer than 2 particles per cell) irrespective of particle size. No significant difference in RAW 264.7 cell association of Au@40k-PEG–MPN nanoparticles or nanocapsules was observed when the size changed from 50 to 100 nm (Figure S11). This is consistent with the previous finding on pure PEG particles, where the PEG particles with diameters of 280, 500, and 1000 nm displayed similar low levels of association with the human monocyte cell line THP-1.[6]

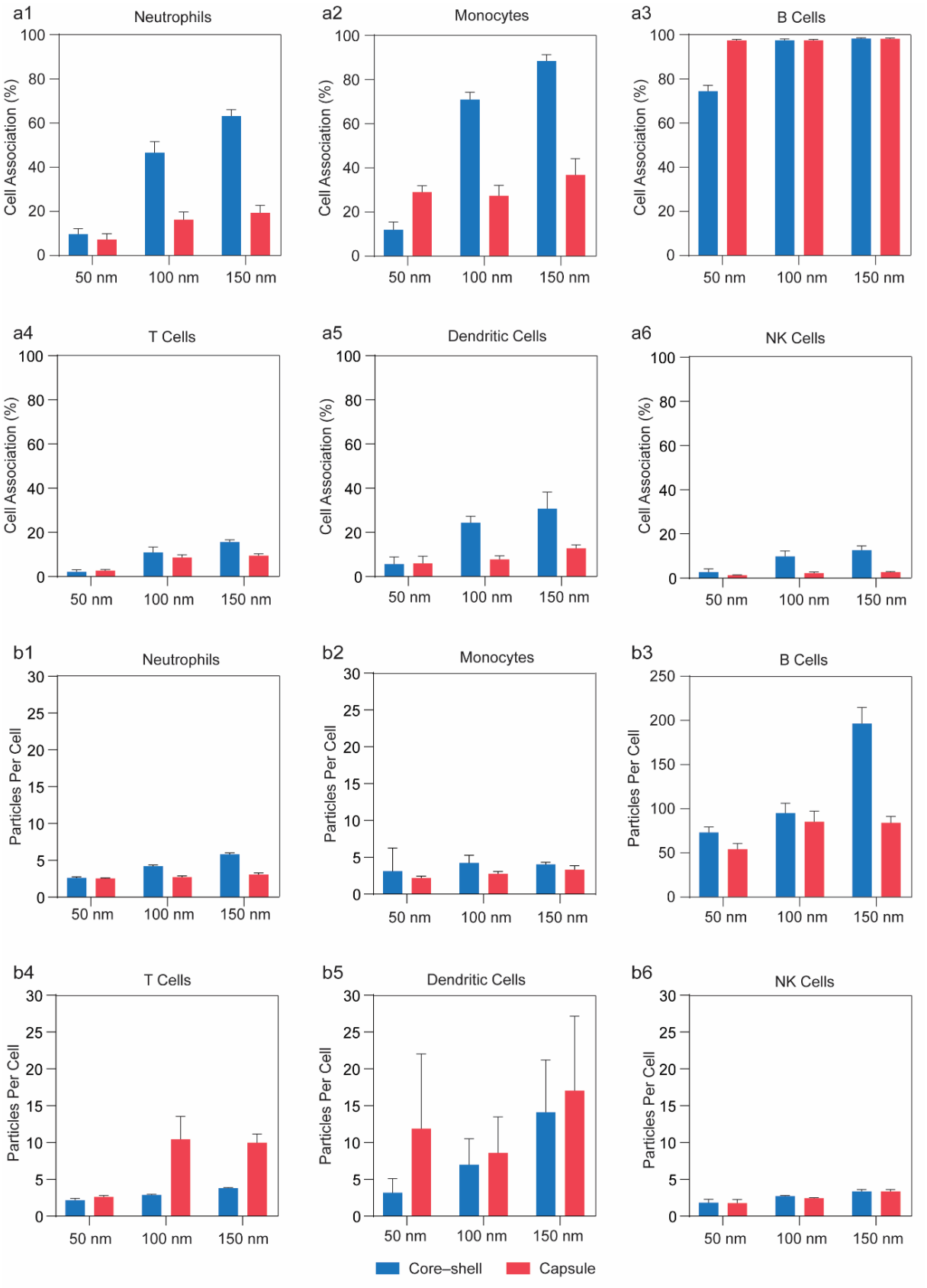
a1
Neutrophils
a2
Monocytes
a3
B Cells
a4
T Cells
a5
Dendritic Cells
a6
NK Cells
b1
Neutrophils
b2
Monocytes
b3
B Cells
b4
T Cells
b5
Dendritic Cells
b6
NK Cells
Cell Association (%)
Particles Per Cell
50 nm
100 nm
150 nm
Core–shell
Capsule

Figure 4. (a) Percentage cell association and (b) median number of particles per cell after 1 h incubation of 50, 100, and 150 nm Au@BDT@40k-PEG–MPN core–shell nanoparticles and Au@40k-PEG–MPN nanocapsules with human whole blood at 37 °C. After incubation, red blood cells were lysed and leukocyte subsets, including neutrophils, monocytes, B cells, T cells, dendritic cells, and NK cells, were labeled by metal-conjugated antibodies and examined by mass cytometry (see gating strategy in Figure S12). Cell association (%) refers to the proportion of leukocytes with positive Au signals above background. The particles per cell count refers to the average number of particles associated with leukocytes, which was calculated based on the median Au signals of the nanoparticles associated with leukocytes. Data are shown as the mean ± SD of three independent experiments, with 50000 leukocytes analyzed for each experimental condition studied. The gating strategy used to identify leukocytes populations and nanoparticles are presented in Figures S12 and S13. Full statistical analysis is presented in Figures S14 and S15.

Ex Vivo Assessment of Particle Interactions with Fresh Human Blood. To further assess the size effect of the Au@BDT@40k-PEG–MPN core–shell nanoparticles and Au@40k-PEG–MPN nanocapsules on their stealth properties, an ex vivo human whole blood assay was performed. Compared with in vitro experiments using immortal cell lines, ex vivo human full blood assays can be used to assess the association of nanoparticles with multiple primary human leukocytes, including granulocytes, monocytes, and lymphocytes, which all play a role in the recognition and elimination of pathogens or foreign materials in the blood. The association of Au@BDT@40k-PEG–MPN core–shell nanoparticles or Au@40k-PEG–MPN nanocapsules with leukocytes, after incubation for 1 h, was investigated using mass cytometry. Both the core–shell nanoparticles and nanocapsules displayed significantly higher association with neutrophils, monocytes, and B cells than with T cells, dendritic cells, and natural killer (NK) cells (Figure 4), which is consistent with

our previous observations of other polymer nanoparticles.[42] Monocytes and neutrophils are expected to have high particle association as their major function is to phagocytose microbes and particulates.[43] The high association with B cells is likely due to the formation of a protein corona on the nanoparticles. Our previous studies have shown that the enrichment of component proteins on nanoparticles can lead to high association with B cells in human blood mediated by complement receptors on B cells.[42,44] In contrast to the in vitro RAW 264.7 cell association results, in which the core–shell particles and capsules of the same size displayed similar cell association, the 100 and 150 nm Au@40k-PEG–MPN nanocapsules showed significantly less association with neutrophils, monocytes, dendritic cells, and NK cells compared with the counterpart core–shell particles of the same size. Furthermore, the influence of particle size on immune cell association became more obvious in the whole blood assay in comparison to the results seen with the cultured macrophage line. Most types of leukocytes (neutrophils, monocytes, B cells, T cells, dendritic cells, and NK cells) demonstrated the same trend: as the size of the Au@BDT@40k-PEG–MPN core–shell nanoparticles increased, particle association with leukocytes also increased significantly (Figure 4a, Figures S14 and S15). As neutrophils make up 40–70% of circulating leukocytes and play a major role in phagocyting foreign matterial,[45] even modest levels of association with nanoparticles can be of importance. The Au@40k-PEG–MPN nanocapsules showed a size-dependent association with neutrophils: as the size of the capsules increased from 50 to 150 nm, neutrophil association and the particles per cell count gradually increased (Figure 4, Figures S14 and S15). Compared with the in vitro RAW 264.7 cell association system, the ex vivo whole blood assay provides a comprehensive environment to assess the stealth properties of a nanoparticle, as it includes all major in vivo blood components, such as all leukocyte subsets, as well as human plasma.

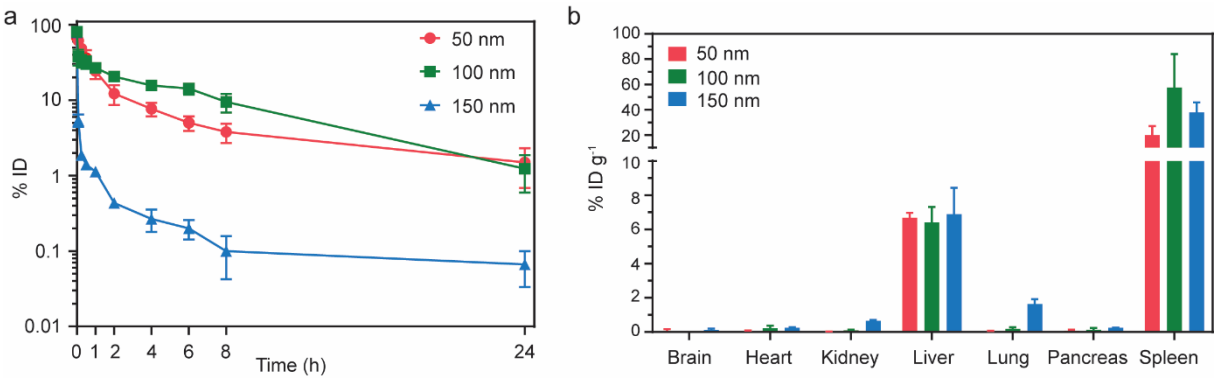

Figure 5. Pharmacokinetics and biodistribution data for Au@40k-PEG–MPN nanocapsules of different sizes after intravenous administration in rats: (a) blood concentration–time profile normalized to percentage of injected dose (%ID) per rat and (b) percentage of injected dose in organs at 24 h normalized for tissue mass (%ID g^{-1}). Values are shown as the mean ± SD (n = 3–4 rats).

In Vivo Blood Circulation and Biodistribution in Rats. Pharmacokinetics and organ distribution studies were conducted in rats to obtain insights into processes leading to the clearance of nanoparticles in vivo. The results of these studies were compared with both the in vitro cell association assay and the ex vivo full blood assay. The 50, 100, or 150 nm Au@40k-PEG–MPN nanocapsules were dispersed in Dulbecco's phosphate-buffered saline (DPBS) at a concentration of 10 μg mL^{-1} and filtered through a 0.22 μm syringe filter. One milliliter of the capsule suspension (approximately 5 μg) was administered intravenously to each rat, and blood samples were taken at multiple time points up to 24 h post-injection. The pharmacokinetic parameters describing the blood profiles were then extracted by PKSolver[46] and compared across groups for the Au@40k-PEG–MPN nanocapsules (Table 1). The elimination half-life values of the 50 and 100 nm Au@40k-PEG–MPN nanocapsules were similar at 4.0 ± 1.6 and 5.2 ± 2.8 h, respectively. Compared to our previous work on PEG–MPN emulsions with a size range of 100−250 nm,[27] the 50 and 100 nm Au@40k-PEG–MPN nanocapsules circulated much longer (4–5 h vs. 50 min) in

vivo, which can be attributed to their smaller and more uniform sizes as well as their hollow structure and near-neutral surface charge. In contrast, the 150 nm Au@40k-PEG–MPN nanocapsules were rapidly cleared from the systemic circulation, with the blood concentration dropping below 5% of the initial injected dose after 5 min (Figures 5a and S16). As consistent with previous studies that have shown that smaller particles are cleared at a slower rate than larger particles,[6,47–49] in the current study, the nanocapsules with a diameter of 100 nm or below significantly outperformed the larger capsules. The relatively shorter circulation time of the 150 nm Au@40k-PEG–MPN nanocapsules correlates to their higher association with leukocytes in the whole blood assay, suggesting that the whole blood assay can serve as an additional surrogate to provide some indications on the in vivo outcomes of nanoparticles.

The high clearance rate (393 ± 40 mL h^{-1}) and steady-state distribution volume, VD_{SS} (359 ± 78 mL), which are derived from the area under the curve (AUC) of the blood concentration–time curve (Figure 5a, Table 1), displayed by the 150 nm Au@40k-PEG−MPN nanocapsules suggest their rapid distribution out of the blood and sequestration by the MPS. Major organs, that is the brain, heart, kidney, liver, lungs, pancreas, and spleen, were recovered to determine Au accumulation after 24 h. As shown in Figure 5b, the Au@40k-PEG–MPN nanocapsules mostly accumulated in the spleen and liver, irrespective of the capsule size studied, which is consistent with previous biodistribution results of other nanoparticle systems.[6,8,36,47] Mechanistically, this result is expected as the liver and spleen are the major organs of the MPS and are responsible for clearing circulating particulates. In addition, as consistent with the more rapid clearance and distribution of the larger 150 nm nanocapsules (Table 1), a trend toward increasing nanocapsule accumulation in the kidney and lungs was also apparent for the larger particles. Although both the liver and spleen showed nanoparticle uptake, the spleen showed higher uptake on a weight basis.

Although it is generally argued that nanoparticle uptake is mainly facilitated by Kupffer cells,[50] it is clear that splenic macrophages also play a significant role,[51,52] although the greater mass of the liver typically results in higher uptake in total by the liver.

Table 1. Overview of calculated pharmacokinetic parameters

Nanocapsule	Elimination half-life $t_{1/2}$ (h)	Clearance (mL h^{-1})	Area under the curve (AUC_{0-t}) (ng h mL^{-1})	Steady-state volume of distribution (VD_{SS}) (mL)
50 nm Au@40k-PEG–MPN	4.0 ± 1.6	21.4 ± 9.3	275 ± 105	133 ± 60
100 nm Au@40k-PEG–MPN	5.2 ± 2.8	9.6 ± 2.5	601 ± 144	65.1 ± 24.8
150 nm Au@40k-PEG–MPN	1.0 ± 0.3	393 ± 40	6.1 ± 0.6	359 ± 78

Conclusion

PEG–MPN core–shell nanoparticles and nanocapsules of different size (50, 100 and 150 nm) were prepared through a one-step assembly process on supramolecular templates. By incorporating a 14 nm AuNP into the nanoparticles, the PEG–MPN nanoparticles and nanocapsules were endowed with a stable signal tracking agent for detection by mass cytometry, thereby enabling whole blood mass cytometry assays and in vivo measurements using ICP-MS. Ex vivo whole blood assay on the PEG–MPN nanocapsules of different sizes revealed that the 50 nm PEG–MPN nanocapsules displayed the least association with most leukocytes. In vivo experiments provided further evidence that the sub-100nm nanocapsules had lower clearance and a longer elimination half-life than their 150 nm counterparts. Overall, the results of the ex vivo human blood assay were

consistent with the in vivo pharmacokinetic data, which suggests the suitability of human blood assays as an additional surrogate to provide insights into the in vivo behaviors of nanoparticles prior to larger animal studies. The reported study represents a new platform to study bio–nano interactions at in vitro, ex vivo, and in vivo levels of detail.

Experimental Section

Materials. 8-Arm-poly(ethylene glycol) succinimidyl succinate of varying molecular weights (8-arm-PEG-NHS, hexaglycerol core; M_w ~10, ~20, and ~40 kDa) were purchased from JenKem Technology (USA). Iron(III) chloride hexahydrate ($FeCl_3 \cdot 6H_2O$), TA, dopamine hydrochloride, MOPS, BDT, anhydrous DMF, triethylamine (TEA), anhydrous dimethyl sulfoxide (DMSO), deuterium oxide (D_2O), and ethylenediaminetetraacetic acid (EDTA), bovine serum albumin (BSA), and fetal bovine serum (FBS) were purchased from Sigma-Aldrich (USA). DPBS and Dulbecco's modified Eagle's medium (DMEM) were purchased from Life Technologies (USA). Paraformaldehyde (PFA, 16% w/v) was purchased from Alfa Aesar. Lysing buffer was purchased from BD Biosciences. For human blood cell phenotyping, purified mouse anti-human CD3 (Clone OKT3), HLA-DR (Clone G46-6), CD45 (Clone HI30), CD56 (Clone NCAM16.2), CD66 (Clone B1.1/CD66), CD16 (Clone 3G8), CD11b (Clone ICRF44), CD19 (Clone HIB19), and CD20 (Clone 2H7) antibodies were purchased from BD Biosciences and purified anti-human CD14 (Clone M5E2) antibody was purchased from BioLegend (USA). Saline was obtained from Baxter Healthcare Pty. Ltd. (Australia). High-purity water (Milli-Q water) with a resistivity greater than 18.2 MΩ cm was obtained from a three-stage Millipore Milli-Q plus 185 purification system (Millipore Corporation, USA).

Synthesis of PEG–Gallol. To synthesize 10k-PEG–gallol, 10 kDa 8-arm-PEG-NHS (100 mg, 10^{-5} mol) and 5-hydroxydopamine hydrochloride (82.3 mg, 4×10^{-4} mol) were dissolved in

degassed anhydrous DMF (1 and 0.5 mL, respectively). The two solutions were then mixed and degassed by argon bubbling. Then, anhydrous TEA (66.5 μL, 4.88×10^{-4} mol) was added to the solution to start the reaction. The mixture was stirred at room temperature under argon degassing for 12 h. The reaction product was purified through dialysis (3500 Da cutoff; Thermo Fisher Scientific, USA) for 3 days against 3 L of degassed Milli-Q water (adjusted to pH 3.5) under nitrogen degassing. The product was then freeze-dried for 1 day and PEG–gallol was obtained as a white powder. To synthesize 20k-PEG–gallol, 20 kDa 8-arm-PEG-NHS (100 mg, 5×10^{-6} mol) and 5-hydroxydopamine hydrochloride (41.1 mg, 2×10^{-4} mol) were used for the reaction. To synthesize 40k-PEG–gallol, 40 kDa 8-arm-PEG-NHS (100 mg, 2.5×10^{-6} mol) and 5-hydroxydopamine hydrochloride (20.6 mg, 1×10^{-4} mol) were used for the reaction.

Synthesis of BDT Particles. The BDT particles were synthesized according to the previous literature.[39] To synthesize BDT particles of 100 nm in diameter, TA solution (1.5 mL, 4 mg mL^{-1} in Milli-Q water) was first added to bicine buffer (12 mL, pH 8.5, 10 mM). The reaction mixture was stirred for 10 min before the addition of BDT solution (1.5 mL, 4 mg mL^{-1} in DMSO). The reaction was further stirred for 12 h. The resulting particles were purified by centrifugation (10000*g*, 10 min) twice to remove the excess complexes. The pellet was resuspended in Milli-Q water for future use. The size of the particles was tuned from 50 to 150 nm by varying the concentration of BDT from 0.25 to 1.0 mg mL^{-1} while fixing the concentration of TA at 0.4 mg mL^{-1}.

Synthesis of Au@BDT Particles. AuNPs of 14 nm in diameter were prepared using a seeded growth method[53] as follows. Typically, sodium citrate aqueous solution (2 mL, 51 mg mL^{-1}) was rapidly injected into boiling aqueous $HAuCl_4$ solution (200 mL, 0.15 mg mL^{-1}) under vigorous

stirring. After boiling for 15 min, the solution was cooled to room temperature, and the resulting particle dispersion was stored at 4 °C for further use.

Encapsulation of a single AuNP in each BDT particle was achieved as follows. A AuNP dispersion (1 mL) was added to bicine buffer (12 mL, pH 8.5, 10 mM), and the reaction mixture was stirred for 10 min. Then, TA solution (1.5 mL, 4 mg mL^{-1}) and BDT solution (1 mL, 4 mg mL^{-1} in DMSO) were added. The reaction was further stirred for 12 h. The resulting particles were purified by centrifugation (10000*g*, 10 min) twice to remove the excess complexes. The pellet was resuspended in Milli-Q water for future use. The size of the particles was tuned from 50 to 150 nm by varying the concentration of BDT from 0.1 to 0.5 mg mL^{-1} while fixing the concentration of TA at 0.38 mg mL^{-1}.

Synthesis of PEG–MPN Core–Shell Nanoparticles and Nanocapsules. Approximately 10^9 BDT particles were suspended in Milli-Q water (300 μL). Then, 0.25 mM PEG–gallol (100 μL; 2.5 mg mL^{-1} 10k-PEG–gallol, 5 mg mL^{-1} 20k-PEG–gallol, or 10 mg mL^{-1} 40k-PEG–gallol) and $FeCl_3 \cdot 6H_2O$ (20 μL, 5 mg mL^{-1}) were added to the particle suspension. The pH of the particle suspension was raised by adding MOPS (300 μL, 20 mM, pH 8.5). The particles were then washed with Milli-Q water for three times. To obtain PEG–MPN nanocapsules, DMF (800 μL) was added to the particle suspension, which was then incubated for 2 h at room temperature. The obtained nanocapsules were spun down and washed with Milli-Q water for three times.

Cell Culture: The murine macrophage cell line RAW 264.7 (American Type Culture Collection, USA) was cultured in DMEM, supplemented with 10% FBS, at 37 °C with 5% CO_2 and 95% relative humidity.

Cell Cytotoxicity Studies. RAW 264.7 cells were seeded onto a 96-well plate at a density of 5000 cells per well. Then, the cells were incubated overnight for cell adhesion on substrates. The

nanoparticles and nanocapsules, that is 100 nm Au@BDT@40k-PEG–MPN, Au@40k-PEG–MPN, and 40k-PEG−MPN, were added to the well at cell-to-particle ratios of 1:250, 1:500, 1:1000, and 1:2000 for 48 h. The cell medium was changed to DPBS containing 3-(4,5-dimethylthiazol-2-yl)-2,5-diphenyltetrazolium bromide (MTT; 0.5 mg mL^{-1}), and the cells were further incubated for 4 h at 37 °C. The medium was then replaced with DMSO (100 μL) to dissolve MTT. The formation of formazan was assessed by measuring the absorbance at 570 nm on an Infinite M200 microplate reader (Tecan, Switzerland).

Cell Association Studies. RAW 264.7 cells were seeded onto a 12-well plate with 2×10^5 cells per well. The seeded cells were incubated overnight to allow cellular adhesion on the substrates. Au@BDT@40k-PEG−MPN nanoparticles and Au@40k-PEG−MPN nanocapsules were incubated with cells at a cell-to-capsule ratio of 1:1000 for 24 h. After incubation, the cells were washed with DPBS gently for three times and then trypsinized with 2×trypsin. Then, the cells were collected and centrifuged at 400*g* for 5 min and washed for three times with DPBS. The cells were then resuspended in 4% PFA with 1/4000 iridium intercalator (Fluidigm). Cell association analysis was performed on a Helios mass cytometer (Fluidigm). Before the test, the cells were washed twice with Milli-Q water to remove PFA and free intercalator and resuspended in Milli-Q water for data acquisition.

Full Blood Assays. Whole blood from healthy volunteers was collected into sodium heparin vacuette tubes (Greiner Bio-One) after obtaining their informed consent in accordance with The University of Melbourne Human Ethics Committee Approval #1443420 and the Australian National Health and Medical Research Council Statement on Ethical Conduct in Human Research. Particles were incubated with blood (200 μL) at 37 °C for 1 h in 5 mL polystyrene tubes (BD Biosciences, San Jose, CA, USA). The leukocyte/particle ratio was around 1:200. After incubation,

1×lysing buffer (4 mL) was added twice to each blood sample to lyse red blood cells. Then, the samples were washed once with flow cytometry staining (FACS) buffer (0.1% BSA, 2 mM EDTA in DPBS). Leukocytes were stained for the mass cytometry analysis using metal-labeled antibodies by incubating with the antibody panel on ice for 40 min. Details of the antibody panel are included in Table S2. Following antibody incubation, each sample was suspended in cisplatin (500 μL, 1/4000 in DPBS) for 5 min to label nonviable leukocytes. The samples were then washed twice with FACS buffer to remove excess cisplatin. Finally, the cell pellets were dispersed in 4% PFA containing 0.025% iridium for at least 2 h to fix cells and to label cells with Ir. Prior to performing the CyTOF analysis, the samples were washed twice with Milli-Q water.

Intravenous Pharmacokinetic Studies. Male Sprague-Dawley rats (250–350 g; n = 4 rats per group) were employed for in vivo studies. Studies were conducted on the basis of previously published procedures.[54] Animal studies were approved by the Monash Institute of Pharmaceutical Sciences Animal Ethics Committee (AEC number: MIPS.18230) and conducted in accordance with the Australian and New Zealand Council for the Care and Use of Animals in Research and Teaching guidelines. Prior to administration of the dose, rats were anaesthetized using isoflurane, and the carotid artery and jugular vein cannulated using polyethylene tubing with outer and inner diameters of 0.96 and 0.58 mm, respectively (Microtube Extrusions, Australia). Rats were subsequently transferred to metabolic cages to recover and were fasted for up to 14 h prior to and for 8 h after dosing. Blank urine and blood (200 μL) were collected prior to dosing. MPNs (5 μg in 1 mL of heparinized saline (10 IU mL^{-1})) were administered as an intravenous infusion (1 mL min^{-1}) via the indwelling jugular cannula. The cannula was then flushed with heparinized saline (300 μL over 30 s) to ensure that any residual formulation was administered. Blood samples (200 μL) were obtained from the carotid artery at time 0 (i.e. immediately at the end of the infusion and

at 5, 15, 30, 60, 120, 240, 360, 480, and 1,440 min after dose administration. Blood samples were collected into tubes containing heparin (5 μL, 1000 IU mL^{-1}) and heparinized saline was flushed through the cannula between samples to maintain cannula patency. Then, aqua regia (1 mL) was added to each blood sample and all the samples were heated to 70 °C for at least 1 h for blood digestion. The samples were topped up to 1.5 mL with Milli-Q water and run on a Nexion 2000 ICP-MS instrument (PerkinElmer) to determine the Au concentration. Pharmacokinetic parameters, including elimination half-life ($t_{1/2}$), clearance, AUC, and VD_{SS}, were computed employing noncompartmental analysis with PKSolver spreadsheet software.[46]

Biodistribution Studies. At the end of the pharmacokinetic studies, i.e. after collection of the last blood sample (24 h), animals were humanely killed by injection with sodium pentobarbital (0.5 mL, 60 mg mL^{-1}) via the jugular cannula. Organs, including the liver, spleen, kidney, lungs, pancreas, heart, and brain, were removed by dissection, weighed, and stored at −20 °C until processed. Aqua regia was added to the organ (5 mL for liver and 2 mL for the remaining organs) and all the organ samples were heated to 80 °C for at least 2 h for organ digestion. Then, the samples were topped up with Milli-Q water (7 mL for liver and 3 mL for the remaining organs) and analyzed by ICP-MS to determine the Au concentration.

Characterization Methods. The chemical structure of the products and efficacy of the modification process were determined by ^{1}H NMR spectroscopy using a 400 MHz Varian INOVA system in D_2O at 25 °C. The efficacy of the modification process was determined by comparing the integral values of the methylene protons in PEG at δ = 3.65 ppm to the aromatic protons in catechol at δ = 6.6–7.0 ppm. TEM analysis was carried out on a Tecnai Spirit (Biosciences) at an operation voltage of 120 kV. Prior to sample analysis, 5 μL of the nanoparticle suspension was dropped onto a plasma-treated copper grid and allowed to air dry. Particle size measurements and

particle per cell counting were performed via NTA on a Malvern NanoSight NS300 instrument fitted with a 405 nm laser (65 mW output). AFM images were acquired on a Cypher ES AFM instrument (Asylum Research, USA) equipped with a Tap 300 cantilever (BudgetSensors) with a spring constant of 40 N m^{-1}. Measurements were performed in tapping mode in air. The nanocapsule suspension was deposited on piranha-cleaned silicon wafers and allowed to dry in air. *Caution: Piranha solution is strongly oxidizing and corrosive! Extreme care should be taken during preparation and use!* UV–Vis absorption spectra of the nanoparticle suspensions recorded within a wavelength range of 400–800 nm were obtained using a Varian Cary 4000 UV–Vis spectrophotometer (Varian, USA). The metal concentration of the Au@PEG–MPN nanocapsules was determined by ICP-MS. ζ-potential measurements were carried out on a Malvern Zetasizer Nano ZS fitted with a 4 mW He-Ne laser (633 nm). XPS analysis was performed on a Kratos Axis ULTRA X-ray photoelectron spectrometer with a 165 mm hemispherical electron energy analyzer. The XPS spectra were processed on CasaXPS.

Minimum Information Reporting in Bio–Nano Experimental Literature (MIRIBEL). The studies conducted herein, including material characterization, biological characterization, and experimental details, conform to the MIRIBEL reporting standard for bio–nano research,[55] and we include a companion checklist of these components in the Supporting Information.

ASSOCIATED CONTENT

Supporting Information. Nanoparticle and nanocapsule characterization (size, ζ-potential, thickness); TEM images of templates and nanocapsules; ^{1}H NMR spectrum; size stability of nanocapsules; XPS patterns of templates, nanoparticles, and nanocapsules; cell viability; calculation of single Au particle intensity in CyTOF studies; cell association with statistical analysis included; gating strategy in whole blood assays; pharmacokinetics data for nanocapsules;

whole blood assay mass cytometry antibody panel; MIRIBEL checklist. The Supporting Information is available free of charge.

AUTHOR INFORMATION

Corresponding Author

*E-mail: skent@unimelb.edu.au.

*Email: chris.porter@monash.edu.

*Email: fcaruso@unimelb.edu.au.

Present Addresses

[†]Present address: School of Health and Biomedical Sciences, RMIT University, Bundoora, Victoria 3083, Australia.

[¶]Present address: Department of NanoEngineering, University of California San Diego, 9500 Gilman Dr., La Jolla, CA, 92093, USA.

Author Contributions

[‡]S.L. and Y.J. contributed equally to this work. S.L. and Y.J. designed the project and drafted the manuscript. S.L. synthesized and characterized the nanoparticles and performed the full blood assay and biodistribution measurements. Y.J. synthesized the PEG–gallol and assisted in the whole process of the work. J.Z. synthesized the BDT particles and assisted with capsule preparation. K.F.N. conducted the rat experiments and the pharmacokinetics and biodistribution analyses. A.J.M. assisted with full blood assay and associated analysis. T.Z. performed the AFM experiments. S.J.K., C.J.H.P., and F.C. contributed to the design of the project and data analysis, supervised the studies, and edited the paper.

ACKNOWLEDGMENT

This research was supported by the Australian Research Council Centre of Excellence in Convergent Bio-Nano Science and Technology (Project No. CE140100036). F.C. acknowledges the award of a National Health and Medical Research Council Senior Principal Research Fellowship (GNT1135806). Y.J. acknowledges the award of an Early Career Researcher Grant from The University of Melbourne (ECR1032020). This work was performed in part at the Materials Characterisation and Fabrication Platform at the University of Melbourne and the Victorian Node of the Australian National Fabrication Facility. The authors acknowledge Dr. Hannah Gabrielle Kelly for helpful discussion and assistance with the whole blood assays.

REFERENCES

(1) Caruso, F. Hollow Capsule Processing through Colloidal Templating and Self-Assembly. *Chem. – Eur. J.* **2000**, *6*, 413–419.

(2) Bollhorst, T.; Rezwan, K.; Maas, M. Colloidal Capsules: Nano- and Microcapsules with Colloidal Particle Shells. *Chem. Soc. Rev.* **2017**, *46*, 2091–2126.

(3) Larrañaga, A.; Lomora, M.; Sarasua, J. R.; Palivan, C. G.; Pandit, A. Polymer Capsules as Micro-/Nanoreactors for Therapeutic Applications: Current Strategies to Control Membrane Permeability. *Prog. Mater. Sci.* **2017**, *90*, 325–357.

(4) Liu, Q.; Liu, H.; Han, M.; Zhu, J.; Liang, Y.; Xu, Z.; Song, Y. Nanometer-Sized Nickel Hollow Spheres. *Adv. Mater.* **2005**, *17*, 1995–1999.

(5) Mora-Huertas, C. E.; Fessi, H.; Elaissari, A. Polymer-Based Nanocapsules for Drug Delivery. *Int. J. Pharm.* **2010**, *385*, 113–142.

(6) Cui, J.; De Rose, R.; Alt, K.; Alcantara, S.; Paterson, B. M.; Liang, K.; Hu, M.; Richardson, J. J.; Yan, Y.; Jeffery, C. M.; Price, R. I.; Peter, K.; Hagemeyer, C. E.; Donnelly, P. S.; Kent, S. J.; Caruso, F. Engineering Poly(ethylene Glycol) Particles for Improved Biodistribution. *ACS Nano* **2015**, *9*, 1571–1580.

(7) Jin, H.; Heller, D. A.; Sharma, R.; Strano, M. S. Size-Dependent Cellular Uptake and Expulsion of Single-Walled Carbon Nanotubes: Single Particle Tracking and A Generic Uptake Model for Nanoparticles. *ACS Nano* **2009**, *3*, 149–158.

(8) Wang, J.; Mao, W.; Lock, L. L.; Tang, J.; Sui, M.; Sun, W.; Cui, H.; Xu, D.; Shen, Y. The Role of Micelle Size in Tumor Accumulation, Penetration, and Treatment. *ACS Nano* **2015**, *9*, 7195–7206.

(9) Talamini, L.; Violatto, M. B.; Cai, Q.; Monopoli, M. P.; Kantner, K.; Krpetic, Z.; Perez-Potti, A.; Cookman, J.; Garry, D.; C, P. S.; Boselli, L.; Pelaz, B.; Serchi, T.; Cambier, S.; Gutleb, A. C.; Feliu, N.; Yan, Y.; Salmona, M.; Parak, W. J.; Dawson, K. A.; Bigini, P. Influence of Size and Shape on the Anatomical Distribution of Endotoxin-Free Gold Nanoparticles. *ACS Nano* **2017**, *11*, 5519–5529.

(10) Decuzzi, P.; Ferrari, M. The Adhesive Strength of Non-Spherical Particles Mediated by Specific Interactions. *Biomaterials* **2006**, *27*, 5307–5314.

(11) Geng, Y.; Dalhaimer, P.; Cai, S.; Tsai, R.; Tewari, M.; Minko, T.; Discher, D. E. Shape Effects of Filaments Versus Spherical Particles in Flow and Drug Delivery. *Nat. Nanotechnol.* **2007**, *2*, 249–55.

(12) Gentile, F.; Chiappini, C.; Fine, D.; Bhavane, R. C.; Peluccio, M. S.; Cheng, M. M.; Liu, X.; Ferrari, M.; Decuzzi, P. The Effect of Shape on the Margination Dynamics of Non-Neutrally Buoyant Particles in Two-Dimensional Shear Flows. *J. Biomech.* **2008**, *41*, 2312–2318.

(13) Thurston, G.; McLean, J. W.; Rizen, M.; Baluk, P.; Haskell, A.; Murphy, T. J.; Hanahan, D.; McDonald, D. M. Cationic Liposomes Target Angiogenic Endothelial Cells in Tumors and Chronic Inflammation in Mice. *J. Clin. Invest.* **1998**, *101*, 1401–1413.

(14) Bai, X.; Wang, S.; Yan, X.; Zhou, H.; Zhan, J.; Liu, S.; Sharma, V. K.; Jiang, G.; Zhu, H.; Yan, B. Regulation of Cell Uptake and Cytotoxicity by Nanoparticle Core under the Controlled Shape, Size, and Surface Chemistries. *ACS Nano* **2020**, *14*, 289–302.

(15) Longmire, M.; Choyke, P. L.; Kobayashi, H. Clearance Properties of Nano-Sized Particles and Molecules as Imaging Agents: Considerations and Caveats. *Nanomedicine* **2008**, *3*, 1–20.

(16) Blanco, E.; Shen, H.; Ferrari, M. Principles of Nanoparticle Design for Overcoming Biological Barriers to Drug Delivery. *Nat. Biotechnol.* **2015**, *33*, 941-951.

(17) Ejima, H.; Richardson, J. J.; Liang, K.; Best, J. P.; van Koeverden, M. P.; Such, G. K.; Cui, J.; Caruso, F. One-Step Assembly of Coordination Complexes for Versatile Film and Particle Engineering. *Science* **2013**, *341*, 154–157.

(18) Ju, Y.; Cortez-Jugo, C.; Chen, J.; Wang, T. Y.; Mitchell, A. J.; Tsantikos, E.; Bertleff-Zieschang, N.; Lin, Y. W.; Song, J.; Cheng, Y.; Mettu, S.; Rahim, M. A.; Pan, S.; Yun, G.; Hibbs, M. L.; Yeo, L. Y.; Hagemeyer, C. E.; Caruso, F. Engineering of Nebulized Metal–Phenolic Capsules for Controlled Pulmonary Deposition. *Adv. Sci.* **2020**, *7*, 1902650.

(19) Ju, Y.; Cui, J.; Müllner, M.; Suma, T.; Hu, M.; Caruso, F. Engineering Low-Fouling and pH-Degradable Capsules through the Assembly of Metal-Phenolic Networks. *Biomacromolecules* **2015**, *16*, 807–814.

(20) Ju, Y.; Cui, J.; Sun, H.; Mullner, M.; Dai, Y.; Guo, J.; Bertleff-Zieschang, N.; Suma, T.; Richardson, J. J.; Caruso, F. Engineered Metal-Phenolic Capsules Show Tunable Targeted Delivery to Cancer Cells. *Biomacromolecules* **2016**, *17*, 2268–2276.

(21) Veronese, F. M.; Pasut, G. PEGylation, Successful Approach to Drug Delivery. *Drug Discovery Today* **2005**, *10*, 1451–1458.

(22) Chow, T.-H.; Lin, Y.-Y.; Hwang, J.-J.; Wang, H.-E.; Tseng, Y.-L.; Wang, S.-J.; Liu, R.-S.; Lin, W.-J.; Yang, C.-S.; Ting, G. Improvement of Biodistribution and Therapeutic Index Via Increase of Polyethylene Glycol on Drug-Carrying Liposomes in an HT-29/luc Xenografted Mouse Model. *Anticancer Res.* **2009**, *29*, 2111–2120.

(23) Harris, J. M.; Chess, R. B. Effect of Pegylation on Pharmaceuticals. *Nat. Rev. Drug Discovery* **2003**, *2*, 214–221.

(24) Zhou, H.; Fan, Z.; Li, P. Y.; Deng, J.; Arhontoulis, D. C.; Li, C. Y.; Bowne, W. B.; Cheng, H. Dense and Dynamic Polyethylene Glycol Shells Cloak Nanoparticles from Uptake by Liver Endothelial Cells for Long Blood Circulation. *ACS Nano* **2018**, *12*, 10130–10141.

(25) Cui, J.; Ju, Y.; Houston, Z. H.; Glass, J. J.; Fletcher, N. L.; Alcantara, S.; Dai, Q.; Howard, C. B.; Mahler, S. M.; Wheatley, A. K. Modulating Targeting of Poly(ethylene Glycol) Particles to Tumor Cells Using Bispecific Antibodies. *Adv. Healthcare Mater.* **2019**, *8*, 1801607.

(26) Cui, J.; Alt, K.; Ju, Y.; Gunawan, S. T.; Braunger, J. A.; Wang, T. Y.; Dai, Y.; Dai, Q.; Richardson, J. J.; Guo, J.; Bjornmalm, M.; Hagemeyer, C. E.; Caruso, F. Ligand-Functionalized Poly(ethylene Glycol) Particles for Tumor Targeting and Intracellular Uptake. *Biomacromolecules* **2019**, *20*, 3592–3600.

(27) Besford, Q. A.; Ju, Y.; Wang, T. Y.; Yun, G.; Cherepanov, P.; Hagemeyer, C. E.; Cavalieri, F.; Caruso, F. Self-Assembled Metal–Phenolic Networks on Emulsions as Low-Fouling and pH-Responsive Particles. *Small* **2018**, *14*, 1802342.

(28) Shao, X.; Zhang, H.; Rajian, J. R.; Chamberland, D. L.; Sherman, P. S.; Quesada, C. A.; Koch, A. E.; Kotov, N. A.; Wang, X. ^{125}I-Labeled Gold Nanorods for Targeted Imaging of Inflammation. *ACS Nano* **2011**, *5*, 8967–8973.

(29) Chen, F.; Hong, H.; Zhang, Y.; Valdovinos, H. F.; Shi, S.; Kwon, G. S.; Theuer, C. P.; Barnhart, T. E.; Cai, W. In Vivo Tumor Targeting and Image-Guided Drug Delivery with Antibody-Conjugated, Radiolabeled Mesoporous Silica Nanoparticles. *ACS Nano* **2013**, *7*, 9027–9039.

(30) Zhang, X.; Chen, F.; Turker, M. Z.; Ma, K.; Zanzonico, P.; Gallazzi, F.; Shah, M. A.; Prater, A. R.; Wiesner, U.; Bradbury, M. S.; McDevitt, M. R.; Quinn, T. P. Targeted Melanoma Radiotherapy Using Ultrasmall ^{177}Lu-Labeled α-Melanocyte Stimulating Hormone-Functionalized Core–Shell Silica Nanoparticles. *Biomaterials* **2020**, *241*, 119858.

(31) Giesen, C.; Wang, H. A.; Schapiro, D.; Zivanovic, N.; Jacobs, A.; Hattendorf, B.; Schüffler, P. J.; Grolimund, D.; Buhmann, J. M.; Brandt, S. Highly Multiplexed Imaging of Tumor Tissues with Subcellular Resolution by Mass Cytometry. *Nat. Methods* **2014**, *11*, 417–422.

(32) Gibson, N.; Holzwarth, U.; Abbas, K.; Simonelli, F.; Kozempel, J.; Cydzik, I.; Cotogno, G.; Bulgheroni, A.; Gilliland, D.; Ponti, J.; Franchini, F.; Marmorato, P.; Stamm, H.; Kreyling, W.; Wenk, A.; Semmler-Behnke, M.; Buono, S.; Maciocco, L.; Burgio, N. Radiolabelling of Engineered Nanoparticles for In Vitro and In Vivo Tracing Applications Using Cyclotron Accelerators. *Arch. Toxicol.* **2011**, *85*, 751–773.

(33) Yin, Y.; Tan, Z.; Hu, L.; Yu, S.; Liu, J.; Jiang, G. Isotope Tracers to Study the Environmental Fate and Bioaccumulation of Metal-Containing Engineered Nanoparticles: Techniques and Applications. *Chem. Rev.* **2017**, *117*, 4462–4487.

(34) AshaRani, P.; Low Kah Mun, G.; Hande, M. P.; Valiyaveettil, S. Cytotoxicity and Genotoxicity of Silver Nanoparticles in Human Cells. *ACS Nano* **2009**, *3*, 279–290.

(35) De Jong, W. H.; Hagens, W. I.; Krystek, P.; Burger, M. C.; Sips, A. J.; Geertsma, R. E. Particle Size-Dependent Organ Distribution of Gold Nanoparticles after Intravenous Administration. *Biomaterials* **2008**, *29*, 1912–1919.

(36) Balasubramanian, S. K.; Jittiwat, J.; Manikandan, J.; Ong, C. N.; Yu, L. E.; Ong, W. Y. Biodistribution of Gold Nanoparticles and Gene Expression Changes in the Liver and Spleen after Intravenous Administration in Rats. *Biomaterials* **2010**, *31*, 2034–2042.

(37) Nold, P.; Hartmann, R.; Feliu, N.; Kantner, K.; Gamal, M.; Pelaz, B.; Huhn, J.; Sun, X.; Jungebluth, P.; Del Pino, P.; Hackstein, H.; Macchiarini, P.; Parak, W. J.; Brendel, C. Optimizing Conditions For Labeling of Mesenchymal Stromal Cells (MSCs) with Gold Nanoparticles: A Prerequisite for In Vivo Tracking of MSCs. *J. Nanobiotechnol.* **2017**, *15*, 24.

(38) Sun, X.; Gamal, M.; Nold, P.; Said, A.; Chakraborty, I.; Pelaz, B.; Schmied, F.; von Pückler, K.; Figiel, J.; Zhao, Y.; Brendel, C.; Hassan, M.; Parak, W. J.; Feliu, N. Tracking Stem Cells and Macrophages with Gold and Iron Oxide Nanoparticles – The Choice of the Best Suited Particles. *Appl. Mater. Today* **2019**, *15*, 267–279.

(39) Zhou, J.; Lin, Z.; Penna, M.; Pan, S.; Ju, Y.; Li, S.; Han, Y.; Chen, J.; Lin, G.; Richardson, J. J.; Yarovsky, I.; Caruso, F. Particle Engineering Enabled by Polyphenol-Mediated Supramolecular Networks. *Nat. Commun.* **2020**, *11*, 4804.

(40) C. Martínez, J.; A. Chequer, N.; L. González, J.; Cordova, T. Alternative Metodology for Gold Nanoparticles Diameter Characterization Using PCA Technique and UV-VIS Spectrophotometry. *Nanosci. Nanotechnol.* **2013**, *2*, 184–189.

(41) Ashby, J.; Pan, S.; Zhong, W. Size and Surface Functionalization of Iron Oxide Nanoparticles Influence the Composition and Dynamic Nature of Their Protein Corona. *ACS Appl. Mater. Interfaces* **2014**, *6*, 15412–15419.

(42) Weiss, A. C. G.; Kelly, H. G.; Faria, M.; Besford, Q. A.; Wheatley, A. K.; Ang, C. S.; Crampin, E. J.; Caruso, F.; Kent, S. J. Link between Low-Fouling and Stealth: A Whole Blood Biomolecular Corona and Cellular Association Analysis on Nanoengineered Particles. *ACS Nano* **2019**, *13*, 4980–4991.

(43) Gustafson, H. H.; Holt-Casper, D.; Grainger, D. W.; Ghandehari, H. Nanoparticle Uptake: The Phagocyte Problem. *Nano Today* **2015**, *10*, 487–510.

(44) Ju, Y.; Kelly, H. G.; Dagley, L. F.; Reynaldi, A.; Schlub, T. E.; Spall, S. K.; Bell, C. A.; Cui, J.; Mitchell, A. J.; Lin, Z.; Wheatley, A. K.; Thurecht, K. J.; Davenport, M. P.; Webb, A. I.;

Caruso, F.; Kent, S. J. Person-Specific Biomolecular Coronas Modulate Nanoparticle Interactions with Immune Cells in Human Blood. *ACS Nano* **2020**, *14*, 15723–15737.

(45) Kolaczkowska, E.; Kubes, P. Neutrophil Recruitment and Function in Health and Inflammation. *Nat. Rev. Immunol.* **2013**, *13*, 159–175.

(46) Zhang, Y.; Huo, M.; Zhou, J.; Xie, S. PKSolver: An Add-in Program for Pharmacokinetic and Pharmacodynamic Data Analysis in Microsoft Excel. *Comput. Methods Programs Biomed.* **2010**, *99*, 306–314.

(47) He, Q.; Zhang, Z.; Gao, F.; Li, Y.; Shi, J. In Vivo Biodistribution and Urinary Excretion of Mesoporous Silica Nanoparticles: Effects of Particle Size and PEGylation. *Small* **2011**, *7*, 271–280.

(48) Sonavane, G.; Tomoda, K.; Makino, K. Biodistribution of Colloidal Gold Nanoparticles after Intravenous Administration: Effect of Particle Size. *Colloids Surf., B* **2008**, *66*, 274–280.

(49) Brinkhuis, R. P.; Stojanov, K.; Laverman, P.; Eilander, J.; Zuhorn, I. S.; Rutjes, F. P.; van Hest, J. C. Size Dependent Biodistribution and SPECT Imaging of ^{111}In-Labeled Polymersomes. *Bioconjug. Chem.* **2012**, *23*, 958–965.

(50) Bertrand, N.; Leroux, J. C. The Journey of a Drug-Carrier in the Body: An Anatomo-Physiological Perspective. *J. Controlled Release* **2012**, *161*, 152–163.

(51) Moghimi, S. M.; Porter, C.; Muir, I.; Illum, L.; Davis, S. Non-Phagocytic Uptake of Intravenously Injected Microspheres in Rat Spleen: Influence of Particle Size and Hydrophilic Coating. *Biochem. Biophys. Res. Commun.* **1991**, *177*, 861–866.

(52) Cataldi, M.; Vigliotti, C.; Mosca, T.; Cammarota, M.; Capone, D. Emerging Role of the Spleen in the Pharmacokinetics of Monoclonal Antibodies, Nanoparticles and Exosomes. *Int. J. Mol. Sci.* **2017**, *18*, 1249.

(53) Zhou, J.; Xiong, Q.; Ma, J.; Ren, J.; Messersmith, P. B.; Chen, P.; Duan, H. Polydopamine-Enabled Approach toward Tailored Plasmonic Nanogapped Nanoparticles: From Nanogap Engineering to Multifunctionality. *ACS Nano* **2016**, *10*, 11066–11075.

(54) Boyd, B. J.; Kaminskas, L. M.; Karellas, P.; Krippner, G.; Lessene, R.; Porter, C. J. Cationic Poly-L-Lysine Dendrimers: Pharmacokinetics, Biodistribution, and Evidence for Metabolism and Bioresorption after Intravenous Administration to Rats. *Mol. Pharmaceutics* **2006**, *3*, 614–627.

(55) Faria, M.; Bjornmalm, M.; Thurecht, K. J.; Kent, S. J.; Parton, R. G.; Kavallaris, M.; Johnston, A. P. R.; Gooding, J. J.; Corrie, S. R.; Boyd, B. J.; Thordarson, P.; Whittaker, A. K.; Stevens, M. M.; Prestidge, C. A.; Porter, C. J. H.; Parak, W. J.; Davis, T. P.; Crampin, E. J.; Caruso, F. Minimum Information Reporting in Bio-Nano Experimental Literature. *Nat. Nanotechnol.* **2018**, *13*, 777–785.

TOC graphic

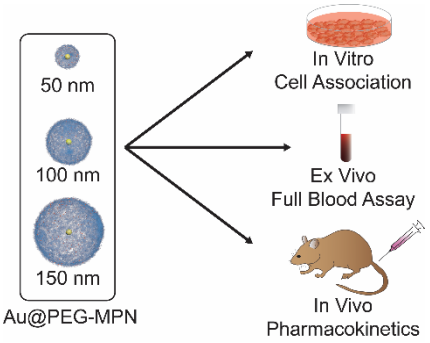
50 nm
100 nm
150 nm
Au@PEG-MPN
In Vitro
Cell Association
Ex Vivo
Full Blood Assay
In Vivo
Pharmacokinetics